

Dynamics of ultrashort pulses near zero dispersion wavelength

Eduard N. Tsoy*

*Centre of Excellence for Ultrahigh-bandwidth Devices for Optical Systems, School of Physics,
University of Sydney, Sydney, New South Wales 2006, Australia*

C. Martijn de Sterke

*Centre of Excellence for Ultrahigh-Bandwidth Devices for Optical Systems, School of Physics,
University of Sydney, Sydney, New South Wales 2006, Australia*

Received May 18, 2006; revised July 24, 2006; accepted July 25, 2006; posted August 4, 2006 (Doc. ID 71033)

The adiabatic dynamics of solitons under the action of third-order dispersion (TOD), the Raman effect, and self-steepening is studied. Using equations that describe the evolution of the pulse parameters, it is shown that the interplay between these effects results in nontrivial pulse dynamics. It is found that positive TOD slows down the self-frequency shift. The theory also describes the eventual suppression of the self-frequency shift in fibers with negative TOD that was recently observed in experiments and described theoretically. The relations of our results to supercontinuum generation are discussed. © 2006 Optical Society of America

OCIS codes: 190.5530, 190.4370, 190.7110, 060.5530.

1. INTRODUCTION

The study of optical pulses propagating near the zero dispersion point (ZDP) of a fiber has at least two important applications. The first one is optical communication systems where this allows one to decrease the power required for generation of stable pulses (solitons).^{1–3} The second application is supercontinuum (SC) generation in various media.^{4,5} This area has attracted much attention after realizing that broad SC can be effectively generated in photonic crystal fibers (PCFs).^{6–8} PCFs have the advantage that the dispersion properties can be engineered in order to meet the requirements. Recently, the nonlinear pulse propagation in antiresonant PCFs near the ZDP was also studied by Fuerbach *et al.*⁹

It is known that SC generation is a complicated process that involves the dynamics of several solitons and dispersive waves (radiation). Now, it is commonly accepted that the main effects that contribute to the SC generation are higher-order dispersion, the Raman and the self-steepening effects, together with a strong interaction between solitons and the phase-locked component of the radiation (see, e.g., Dudley *et al.*⁸). Therefore, it is interesting to study how these effects change the dynamics of a *single* soliton.

The influence of these higher-order effects individually has been studied extensively.^{10–16} The simultaneous action of the effects mentioned on the pulse propagation was studied by many authors^{17–23} (see also Refs. 1–3). However, there is still a need for an analytical description of the dynamics. For example, Zhao and Bourkoff¹⁷ present mainly numerical results. The study by Frantzeskakis *et al.*¹⁸ is based on a search of exact solutions of the governing equation. Ankiewicz¹⁹ considers the influence of different effects, including Raman scattering, higher-order dispersion, two-photon absorption and saturation of non-

linearity but does not analyze the interplay of the effects in the detail. Golles *et al.*²⁰ use the inverse scattering transform method in order to find the evolution of solitons bounded in a multisoliton state. The paper by Karpman²¹ concentrates on the properties of the radiation emitted by the soliton. Both the soliton dynamics and the radiation are considered by Biancalana *et al.*²³ These authors used the complete response function of the Raman effect,¹⁴ which complicates the analysis. Also, the self-steepening effect was omitted by Biancalana *et al.*²³ These authors mainly studied the case of negative third-order dispersion (TOD) aiming to explain the suppression of the Raman self-frequency shift observed in the experiment.²² In our study, we use the simplified form of the Raman response^{1,13} and focus on the soliton's adiabatic dynamics. The advantage of such an approach is that, in many cases, it allows us to obtain *explicit* expressions for the soliton parameters. We also analyze both signs of TOD.

The paper is organized as follows. In Section 2, we present the basic equation that describes the propagation of ultrashort pulses. The method of analysis and the range of applicability are outlined in Section 3. The separate influence of Raman scattering and third-order dispersion, as well as the combined action of these effects together with self-steepening, are studied in Section 4. In particular, it is shown how TOD affects the Raman self-frequency shift.^{22,23} Section 5 provides a summary of the results and a conclusion.

2. DESCRIPTION OF THE PROBLEM

The basic equation that describes the propagation of ultrashort pulses in optical fibers near the ZDP has the form of the perturbed nonlinear Schrödinger equation (NLSE)^{1–3,13}:

$$i \frac{\partial \psi}{\partial z} - \frac{\beta_2}{2} \frac{\partial^2 \psi}{\partial t^2} + \gamma |\psi|^2 \psi = \frac{i\beta_3}{6} \frac{\partial^3 \psi}{\partial t^3} - \gamma \left[iT_S \frac{\partial}{\partial t} (|\psi|^2 \psi) - T_R \psi \frac{\partial |\psi|^2}{\partial t} \right] \equiv R(\psi). \quad (1)$$

Here $\psi(t, z)$ is the slowly varying envelope of the field at the frequency ω_0 , z is the propagation distance, $t = t' - z/v_g$ is the retarded time, where t' is the real time and v_g is the group velocity. Parameters $\beta_2(\omega_0)$ and $\beta_3(\omega_0)$ are the coefficients of the second- and the third-order dispersion, respectively. In this paper, we assume that the operating frequency ω_0 is in the anomalous dispersion region, $\beta_2(\omega_0) < 0$, and that the Kerr nonlinearity coefficient γ is positive. T_S and T_R are characteristic time scales of the self-steepening and Raman effects, respectively. In standard silica fibers, for wavelength $\lambda = 1.55 \mu\text{m}$, one can take $T_R \sim 1\text{--}5$ fs and $T_S \sim 2$ fs, so that for pulses below ~ 1 ps, these effects become important.¹ Here, we restrict ourselves to TOD; however, inclusion of the higher-order terms into the analysis is straightforward.

The full description of the Raman effects in fibers involves using the response function $F(t)$, so that the factor $T_R \partial |\psi|^2 / \partial t$ of the Raman term in Eq. (1) needs to be replaced by the convolution J of $F(t)$ and the field intensity.^{1,3,14} The n th term of the J expansion is proportional to $J_n \equiv (\Phi_n/n!) \partial^n |\psi|^2 / \partial t^n$, $n \geq 1$ where $\Phi_n \equiv d^n \Phi(\omega) / d\omega^n$ at $\omega=0$ and $\Phi(\omega)$ is the Fourier transform of $F(t)$. One can estimate $J_n \sim (\Phi_n/n!) p/w^n$, where p and w are the pulse peak power and width, respectively. Therefore, the condition for replacing J by J_1 can be written as

$$w \gg w_c(n) \equiv [\Phi_n/(n! \Phi_1)]^{1/(n-1)}, \quad n > 1.$$

For the parameters of $F(t)$ of silica fibers¹⁴ with $\tau_1 = 12.2$ fs, $\tau_2 = 32$ fs, and $f = 0.18$, the characteristic scale $w_c(n)$ is estimated as $w_c(n) \leq 15$ fs. Therefore, if the pulse width is much larger than 15 fs, then one can use the approximate expression for the Raman effect as in Eq. (1). The parameter T_R is defined as¹²⁻¹⁴ $T_R = 2f\tau_1^2\tau_2(\tau_1^2 + \tau_2^2)^{-1}$.

It is known that Eq. (1) without perturbations ($R=0$) supports the propagation of stable pulses or solitons. The presence of additional effects changes the parameters of solitons and also results in emission of dispersive waves by solitons. The main aim of the present work is to find the variation of soliton parameters under the action of the TOD, Raman effect, and self-steepening. We do not include in consideration either the radiation or interaction between a soliton and radiated waves. Therefore, our approach is valid while the energy losses of the soliton to the emitted waves are small.

3. METHOD

We consider a pulse in the form of a hyperbolic secant function:

$$\psi(t, z) = A \operatorname{sech}\left(\frac{t - t_c}{w}\right) \exp\{i[\phi + b(t - t_c) + \mu(t - t_c)^2]\}, \quad (2)$$

where $A(z)$, $w(z)$, and $t_c(z)$ are the amplitude, width, and maximum position of the pulse, respectively, $\phi(z)$ is the phase shift, $b(z)$ is the linear phase (frequency shift) coefficient, and $\mu(z)$ is the chirp parameter. The phase in Eq. (2) is expanded up to the second order. The derivative $t_{c,z} = dt_c/dz$ accounts for the deviation of the pulse velocity from the group velocity due to the additional effects. In real coordinates, the pulse velocity v is given by

$$v = \frac{v_g}{1 - t_{c,z} v_g} \approx v_g(1 + t_{c,z} v_g); \quad (3)$$

below we refer to $t_{c,z}$ as to the *relative velocity*. The actual center frequency ω of the pulse is $\omega = \omega_0 - b$.

We assume that the pulse shape does not change while the pulse parameters vary during propagation. To find the evolution of the parameters, we use the method of moments.²⁴ We start from the integral characteristics of the field, namely, the energy Q and momentum P ,

$$Q = \int_{-\infty}^{\infty} |\psi|^2 dt, \quad P = \frac{1}{2} \int_{-\infty}^{\infty} (\psi \psi_t^* - \psi_t^* \psi) dt, \quad (4)$$

and higher-order moments²⁴:

$$I_1 = \int_{-\infty}^{\infty} t |\psi|^2 dt, \\ I_2 = \int_{-\infty}^{\infty} (t - t_c)^2 |\psi|^2 dt, \\ I_3 = \int_{-\infty}^{\infty} (t - t_c) (\psi^* \psi_t - \psi \psi_t^*) dt, \quad (5)$$

where $t_c(z) = I_1/Q$, provided that $|\psi|$ is symmetric function of $t - t_c$. Integrals I_1 and I_2 are the center and the dispersion of the energy distribution in the pulse, while I_3 characterizes the asymmetry of the momentum distribution.

For arbitrary perturbation R of the NLSE, cf. Eq. (1), one can derive the equations for the generalized moments²⁴ (see also Tsoy *et al.*²⁵):

$$\frac{dQ}{dz} = i \int_{-\infty}^{\infty} (\psi R^* - \psi^* R) dt,$$

$$\frac{dP}{dz} = -i \int_{-\infty}^{\infty} (\psi_t R^* + \psi_t^* R) dt,$$

$$\frac{dI_1}{dz} = -i\beta_2 P + i \int_{-\infty}^{\infty} t (\psi R^* - \psi^* R) dt,$$

$$\frac{dI_2}{dz} = i\beta_2 I_3 + i \int_{-\infty}^{\infty} (t - t_c)^2 (\psi R^* - \psi^* R) dt,$$

$$\begin{aligned} \frac{dI_3}{dz} = & 2P \frac{dt_c}{dz} - i \int_{-\infty}^{\infty} (2\beta_2 |\psi_t|^2 + \gamma |\psi|^4) dt \\ & + 2i \int_{-\infty}^{\infty} (t - t_c) (\psi_t R^* + \psi_t^* R) dt \\ & + i \int_{-\infty}^{\infty} (\psi R^* + \psi^* R) dt, \end{aligned} \quad (6)$$

where the asterisk means the complex conjugate and R is the perturbation to the NLSE [cf. Eq. (1)]. These equations are quite general and can be applied to the NLSE with any perturbations.

The method described does not explicitly include the linear waves. However, as shown by Kath and Smyth,²⁶ to some extent, the soliton chirp models the interaction of the soliton with the radiation. For the validity of the method, it is necessary that the perturbation R is small (see below) and that the amount of emitted radiation is modest.

We check the results of the approximate analysis with those from the numerical simulations of Eq. (1). In numerical modeling, we use the dimensionless form of Eq. (1). For this purpose, we introduce

$$u(\bar{z}, \bar{t}) = \frac{\psi(z, t)}{\psi_{cs}}, \quad \bar{z} = \frac{z}{z_{cs}}, \quad \bar{t} = \frac{t}{t_{cs}}, \quad (7)$$

where t_{cs} is a time scale of the input pulse, and the characteristic scales z_{cs} and ψ_{cs} are defined as

$$z_{cs} = \frac{t_{cs}^2}{|\beta_2|}, \quad \psi_{cs} = \frac{1}{t_{cs}} \left(\frac{|\beta_2|}{\gamma} \right)^{1/2}. \quad (8)$$

Then, the corresponding NLSE has the form

$$\begin{aligned} i \frac{\partial u}{\partial \bar{z}} - \frac{\text{sgn}(\beta_2)}{2} \frac{\partial^2 u}{\partial \bar{t}^2} + |u|^2 u = & i \frac{\bar{\beta}_3}{6} \frac{\partial^3 u}{\partial \bar{t}^3} \\ & - \left[i \bar{T}_S \frac{\partial}{\partial \bar{t}} (|u|^2 u) - \bar{T}_R u \frac{\partial |u|^2}{\partial \bar{t}} \right], \end{aligned} \quad (9)$$

where

$$\bar{\beta}_3 = \frac{\beta_3}{|\beta_2| t_{cs}}, \quad \bar{T}_S = \frac{T_S}{t_{cs}}, \quad \bar{T}_R = \frac{T_R}{t_{cs}}. \quad (10)$$

One could take $t_{cs} = w_0$, so that the dimensionless width of the input pulse equals unity. However, in numerical simulations, we also vary the ratio w_0/t_{cs} in order to study the dependence on the pulse width. We also assume that the influence of the additional effects is small, so that $\bar{\beta}_3, \bar{T}_S$, and $\bar{T}_R \sim \epsilon \ll 1$. In the sections below, we omit the bar sign of the dimensionless variables where it does not cause confusion.

4. RESULTS

For the particular perturbations in Eq. (1), one can obtain from Eqs. (6) the set of equations for the soliton parameters,

$$Q_z = 0, \quad (11)$$

$$b_z = \frac{2Q\gamma}{15w^3} (2T_R + 5T_S \mu w^2), \quad (12)$$

$$t_{c,z} = -\beta_2 b + \frac{\beta_3}{6w^2} (1 + 3b^2 w^2 + \pi^2 \mu^2 w^4) + \frac{\gamma T_S Q}{2w}, \quad (13)$$

$$w_z = -2\hat{\beta}_2 \mu w, \quad (14)$$

$$\mu_z = \frac{1}{\pi^2 w^4} [-2\hat{\beta}_2 (1 - \pi^2 \mu^2 w^4) - \gamma Q w (1 - T_S b)], \quad (15)$$

where $\hat{\beta}_2 = \beta_2 - \beta_3 b$ is the group velocity dispersion at the soliton frequency. Note that the effects included in Eq. (1) do not change the pulse energy,

$$Q = 2A^2(z)w(z) = 2A_0^2 w_0 = \text{const}, \quad (16)$$

where $A_0 = A(0)$ and $w_0 = w(0)$. Of course, this does not account for loss of the energy due to the radiation of dispersive waves.

By combining Eqs. (14) and (15), we find

$$\begin{aligned} w_{zz} = & \frac{2\hat{\beta}_2}{\pi^2} \left[\frac{2\hat{\beta}_2}{w^3} + \frac{\gamma Q (1 - T_S b)}{w^2} \right] \\ & + \frac{\beta_3 \gamma Q w_z}{15\hat{\beta}_2^2 w^3} (5T_S w w_z - 4\hat{\beta}_2 T_R). \end{aligned} \quad (17)$$

We use Eq. (17) for the analysis of the dynamics.

In the presence of the self-steepening effect only, $T_S \neq 0$ and $\beta_3 = T_R = 0$, the corresponding NLSE can be reduced to the derivative NLSE (see, e.g., Ref. 3, chap. 6). The derivative NLSE is integrable by the inverse scattering transform method.²⁷ The derivative NLSE allows for the propagation of robust solitons similar to the pure NLSE. Therefore, we do not consider this case. The details of the dynamics and corresponding references can be found in Ref. 3.

In the following subsections first we briefly review the main characteristics of the pulse dynamics in the unperturbed case $T_S = T_R = \beta_3 = 0$. Though this is well known (see, e.g., Ref. 1) this description is useful for a better understanding of the influence of the higher-order effects. Then, we consider the influence of TOD and the Raman effect separately. We compare the results obtained from Eqs. (11)–(15) with those known from the literature.^{11,12,15,19} This justifies our approach and defines the regions of validity in the parameter space. Then, we consider the combination of the TOD and Raman effect (or self-steepening). Finally, we analyze the general case when all three perturbations act simultaneously.

A. Unperturbed Nonlinear Schrödinger Equation, β_3

$$= T_S = T_R = 0$$

Here we have $Q_z = b_z = 0$, and if $b_0 \equiv b(0) = 0$, then $t_{c,z} = 0$. The equation for w is

$$w_{zz} = \frac{2\beta_2}{\pi^2} \left(\frac{2\beta_2}{w^3} + \frac{\gamma Q}{w^2} \right) \equiv -\frac{\partial U}{\partial w}, \tag{18}$$

where

$$U = \frac{2}{\pi^2} \left(\frac{\beta_2^2}{w^2} + \frac{\gamma Q \beta_2}{w} \right). \tag{19}$$

Equation (18) corresponds to the motion of an equivalent classical particle in the potential U . This equation is the same as that obtained from the variational approach²⁸ based on the Lagrangian of Eq. (1). As pointed out by Abdullaev and Caputo,²⁹ the potential U is that of the classical Kepler problem.³⁰ Equation (18) has a conservative quantity, which is the energy of the equivalent particle

$$E = \frac{w_z^2}{2} + \frac{2}{\pi^2} \left(\frac{\beta_2^2}{w^2} + \frac{\gamma Q \beta_2}{w} \right). \tag{20}$$

For $\beta_2 < 0$, the potential U has a single minimum at

$$w_s = -\frac{2\beta_2}{\gamma Q}. \tag{21}$$

This stationary point corresponds to a fundamental soliton solution of the unperturbed Eq. (1), which propagates without variation of its shape. Equation (21) together with Eq. (16) also provide a relation between the amplitude A_s and width w_s of the fundamental soliton:

$$A_s w_s = \sqrt{\frac{-\beta_2}{\gamma}}. \tag{22}$$

This relation, which here follows from the moment method analysis, coincides with the exact result.¹

If $w_0 \neq w_s$, or in other words, if A_0 and w_0 do not satisfy Eq. (22), then for $E < 0$, as follows from Eq. (18), w oscillates near the stationary point. In fact, as shown by Satsuma and Yajima,³¹ these oscillations are damped, so that w asymptotically approaches a value close to that given by Eq. (21). The damping is because the soliton radiates dispersive waves, adjusting its form. This damping should be remembered while comparing the approximate results with the actual dynamics of the system.

If $E > 0$, then w diverges upon propagation and the pulse decays dispersively. In particular, for a given value of Q , narrow pulses with $w_0 < w_s/2$ and $c_0 = 0$ decay, a result that coincides with the exact theory for the unperturbed NLSE.

B. Case $\beta_3 \neq 0$ and $T_S = T_R = 0$

In this case, Eqs. (11)–(15) reduce to

$$Q_z = b_z = 0, \tag{23}$$

$$t_{c,z} = -\beta_2 b + \frac{\beta_3}{6w^2} (1 + 3b^2 w^2 + \pi^2 \mu^2 w^4), \tag{24}$$

$$w_{zz} = \frac{2\hat{\beta}_2}{\pi^2} \left(\frac{2\hat{\beta}_2}{w^3} + \frac{\gamma Q}{w^2} \right), \tag{25}$$

and μ is found from w by using Eq. (14). Equation (23) implies that b is constant. Actually, as shown by Elgin *et al.*,¹⁵ the frequency shift b changes with z ; however, the variations are of order $O(\epsilon^2)$. Equation (25) with substitution $\hat{\beta}_2 \rightarrow \beta_2$ has the same form as Eq. (18). Therefore, regarding the pulse width w and chirp μ , the TOD just redefines the dispersion parameter from β_2 to $\hat{\beta}_2$. The linear dependence of $\hat{\beta}_2$ on b arises because we consider TOD only and thus a linear dependence of the second-order dispersion on ω . Hence, for $w(0) \approx w_s$, one has $w(z) \rightarrow w_s$ and $\mu(z) \rightarrow 0$ after a transient process. When $b(0) = 0$, we find that the relative velocity [cf. Eq. (3)] is

$$t_{c,z} \approx \frac{\beta_3}{6w_s^2} = \frac{\beta_3 \gamma^2 Q^2}{24\hat{\beta}_2^2}, \quad z \rightarrow \infty. \tag{26}$$

Equation (26) shows that shorter (longer) pulses have larger group velocities for $\beta_3 > 0$ ($\beta_3 < 0$). This result is in agreement with the work by Elgin *et al.*,¹⁵ who also present a detailed analysis of the TOD influence including the properties of the radiation emitted by the soliton.

C. Case $T_R \neq 0$ and $\beta_3 = T_S = 0$

As seen from Eqs. (11)–(15), the parameter T_R is present only in the equation for b . Therefore, the dynamics of w and μ is the same as that in the *unperturbed* case. The soliton parameters tend to those of the fundamental soliton: $w \rightarrow w_s$, $c \rightarrow 0$, and $A \rightarrow Q/w_s$. At the same time, the Raman effect generates a frequency shift, the evolution of which is found from

$$b_z = \frac{4\gamma T_R Q}{15w^3}. \tag{27}$$

For the fundamental soliton $w = w_s$, the last equation can be written as

$$b_z = \frac{8T_R |\beta_2|}{15w_s^4}. \tag{28}$$

The frequency shift b increases linearly on the propagation distance, and it is inversely proportional to the fourth power of the pulse width. This dependence agrees with earlier results obtained by other authors.^{12,19} The relative velocity changes linearly with z as follows from Eq. (13).

D. Case $\beta_3 \neq 0$, $T_S \neq 0$, and $T_R = 0$:

The dynamical equations can now be written as

$$b_z = \frac{\gamma T_S Q w_z}{3\hat{\beta}_2 w^2}, \quad \mu = -\frac{w_z}{2\hat{\beta}_2 w}, \tag{29}$$

$$w_{zz} = \frac{2\hat{\beta}_2}{\pi^2} \left[\frac{2\hat{\beta}_2}{w^3} + \frac{\gamma(1 - T_S b)Q}{w^2} \right] + \frac{\beta_3 \gamma T_S Q}{3\hat{\beta}_2^2} \left(\frac{w_z}{w} \right)^2. \tag{30}$$

The first of Eqs. (29) results in the conservation law:

$$\frac{d}{dz} \left[\beta_2 b - \beta_3 \frac{b^2}{2} - \frac{\gamma T_S Q}{3w} \right] = 0. \quad (31)$$

This allows one to express the frequency shift b in terms of the width variation, giving:

$$b \approx b_0 + \frac{\gamma T_S Q}{3\beta_2} \left(\frac{1}{w} - \frac{1}{w_0} \right), \quad (32)$$

where $b_0 = b(0)$ and $w_0 = w(0)$.

Equation (30) has a stationary point at $w_z \sim \mu = 0$ and $w = w_s$ where

$$w_s = - \frac{2\hat{\beta}_2}{\gamma(1 - T_S b)Q}. \quad (33)$$

If one takes $b_0 = \mu_0 = 0$ and $w_0 \approx w_s$, then $w(z)$, $\mu(z)$, and $b(z)$ oscillate near stationary values. Therefore, for such initial conditions, the dynamics of $w(z)$ is similar to the unperturbed case with a slight variation of the stationary point according to Eq. (33).

E. Case $\beta_3 \neq 0$, $T_R \neq 0$, and $T_S = 0$

The evolution of b is described by Eq. (27), while the equation for w is now written as

$$w_{zz} = \frac{2\hat{\beta}_2}{\pi^2} \left[\frac{2\hat{\beta}_2}{w^3} + \frac{\gamma Q}{w^2} \right] - \frac{4}{15} \frac{\beta_3 \gamma T_R Q w_z}{\hat{\beta}_2 w^3}. \quad (34)$$

Ignoring the last term in Eq. (34), one can write the energy of the equivalent particle (cf. Subsection 4.A):

$$E = \frac{w_z^2}{2} + \frac{2\hat{\beta}_2}{\pi^2} \left[\frac{\hat{\beta}_2}{w^2} + \frac{\gamma Q}{w} \right]. \quad (35)$$

Similar to the unperturbed case discussed in Subsection 4.A, if $E_0 = E(z=0) < 0$ ($E_0 > 0$), then the dynamics of w has (has not) a bound state. However, inclusion of the last term in Eq. (34) can change this condition so that the initially bounded dynamics of w can become unbound. The last term in Eq. (34) can be considered as a w -dependent amplification (dissipation) for $\beta_3 T_R / \hat{\beta}_2 > 0$ (< 0).

In this subsection, we consider $T_R > 0$ that corresponds to optical fibers. However, Eqs. (27) and (34) are invariant with respect to the transformation $T_R \rightarrow -T_R$, $\beta_3 \rightarrow -\beta_3$, and $b \rightarrow -b$; therefore the analysis below can be applied formally for the case $T_R < 0$ too.

1. Case $\beta_3 > 0$

As follows from Eq. (27), for $T_R > 0$, b is always an increasing function of z , since the Raman effect induces always the red frequency shift. Then, Eq. (34) can be interpreted as a motion in a slowly varying potential with the additional action of dissipation or amplification. The minimum of the potential,

$$w_s = -2\hat{\beta}_2 / (\gamma Q), \quad (36)$$

increases with z because of the variation of $\hat{\beta}_2$. For $\beta_3 > 0$, assuming also $b > 0, |\hat{\beta}_2|$ as well as w_s increase. Therefore, $w(z)$ is an oscillating function of z with increasing average value defined by Eq. (36).

For initial pulses close to the fundamental soliton, one can substitute w_s from Eq. (36) instead of w to Eq. (27). Then, the evolution of the frequency shift is written as

$$b = \frac{1}{\beta_3} \left[\beta_2 + \left(\hat{\beta}_{2,0}^4 + \frac{2}{15} \beta_3 T_R \gamma^4 Q^4 z \right)^{1/4} \right], \quad (37)$$

where $\hat{\beta}_{2,0} \equiv \hat{\beta}_2(z=0) = \beta_2 - \beta_3 b_0 < 0$, and which is valid while b is such that $\hat{\beta}_2 \leq 0$. The evolution of the soliton velocity is found from that of b [see Eq. (13)],

$$t_{c,z} \approx -\beta_2 b + \frac{\beta_3}{2} b^2, \quad (38)$$

which is the relative group velocity of linear waves of the NLSE (1). The parameters b and w_s approach $\sim z^{1/4}$ at large z . Therefore, positive TOD decelerates the variation of the frequency shift as compared with the linear z dependence of the Raman shift for $\beta_3 = 0$ (see Subsection 4.C). The qualitative explanation is as follows. The Raman redshift at $\beta_3 > 0$ moves the soliton frequency *away* from the ZDP so that the absolute value $|\hat{\beta}_2|$ of the group velocity dispersion increases. This results in an increase of the soliton width, c.f. Eq. (36). This change, in turn, decreases the rate of the frequency shift variation via Eq. (27). As we shall see below, the frequency shift dynamics has a more dramatic change for $\beta_3 < 0$, consistent with Refs. 22 and 23.

Figure 1 shows the dependencies of w and b on z . Curves correspond to the numerical simulations of Eqs. (27) and (34) in Fig. 1(a) and to Eq. (37) in Fig. 1(b), while points are from numerical simulations of Eq. (9). The pa-

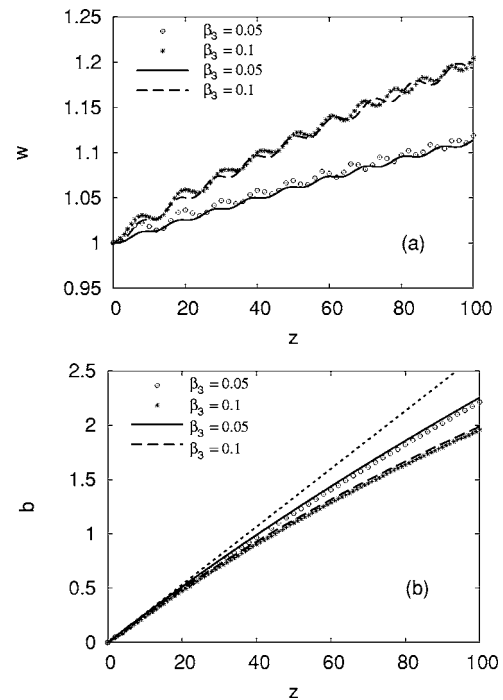


Fig. 1. Dependence of (a) soliton width and (b) frequency shift on z for $\beta_3 > 0$. Solid and dashed curves correspond to (a) numerical simulations of Eqs. (27) and Eqs. (34), (b) Eq. (37), while points are from numerical simulations of Eq. (9). The dotted line in (b) is the dependence for $\beta_3 = 0$. Parameters are $T_R = 0.05$ and $A_0 = w_0 = 1$.

parameter b is calculated at the pulse center by using the phases of the two points adjacent to the soliton center. The initial condition corresponds to the fundamental soliton, i.e., $w_0 = w_s$ so that the effective particle is at the potential minimum at $z=0$. The width $w(z)$ follows the minimum position that increases with z [see Eq. (36)]. Small oscillations of w near w_s mean that the variation of the potential is not completely adiabatic. The frequency shift b increases as described by Eq. (37) but slower than the linear dependence of b for $\beta_3=0$ [dotted line in Fig. 1(b)]. Note the good agreement of numerical results with theoretical predictions discussed above. When the initial condition is not the fundamental soliton, then the oscillations of w have a much larger amplitude, and the numerical results deviate more from the theoretical ones.

2. Case $\beta_3 < 0$

For $\beta_3 < 0$, the Raman effect, that always shifts the spectrum to longer wavelengths, moves the soliton frequency toward the ZDP. The decrease of $|\hat{\beta}_2|$ results in a decrease of the soliton width. Then, as follows from Eqs. (27) and (34), at some distance, the effective dispersion becomes normal, $\hat{\beta}_2 > 0$. For Eq. (34), this means that the stationary point of the potential disappears, and the potential is a decreasing function of w . Then, the pulse decays dispersively so that its width is predicted to increase indefinitely. The frequency shift rate increases initially. Then, after the threshold distance, the rate decreases, and the frequency shift saturates as follows from Eq. (27) because $b_z \approx 0$ for large w . As we see below, the numerical simulations of Eq. (1) give a slightly different behavior.

One can estimate the threshold length z_{th} , where pulses start to decay, from the condition $\hat{\beta}_2 = 0$ or from Eq. (37). The expression in parentheses in Eq. (37) turns to zero at

$$z_{th} = - \frac{15 \hat{\beta}_{2,0}^A}{2 \beta_3 T_R \gamma^A Q^4}, \tag{39}$$

a result that is valid for pulses close to the fundamental soliton. Equations (36)–(38) are valid for $\beta_3 < 0$ as well, provided that $z < z_{th}$.

The evolution of w and b with z for different values of β_3 is presented in Fig. 2. The values of b found from Eq. (37) are not shown, since the equation is valid for $z < z_{th}$, however, for that region, these values are very close to those obtained from numerical solutions of Eqs. (27) and (34). The theory [curves in Fig. 2(a)] predicts a decrease of w and then a sharp increase. The frequency shift [solid and dashed curves in Fig. 2(b)] initially increases faster than the linear dependence for $\beta_3=0$ [dotted line in Fig. 2(b)]. Then, our theory predicts that the frequency shift saturates at a value such that $\hat{\beta}_2 > 0$. Actually, numerical simulations [points in Fig. 2(a)] of Eq. (9) show that the pulse width decreases initially, and then after the threshold, it gradually increases. Also, in contrast to the theory, the effective dispersion at the soliton frequency is still negative after the threshold. The theory and numerical simulations differ because the pulse loses the energy to resonant radiation²² near the threshold. For the same reason, the theory overestimates the asymptotic value of

the frequency shift. Numerical simulations of Eq. (9) also show that parameter Q , corresponding to soliton energy, is almost constant at $z < z_{th}$ as given by Eq. (11); Q decreases considerably at $z > z_{th}$. Nevertheless, the theory provides a correct description of the initial stage of the dynamics for $\beta_3 < 0$. Moreover, it gives reasonable values of the threshold distance, Eq. (39).

A typical example of the field evolution is shown in Fig. 3. The pulse propagates to the right-hand side along the t axis. At $z \approx 90$, the pulse narrows and starts to generate radiation (cf. Ref. 22). The theoretical value, for the threshold calculated from Eq. (39) for the parameters in Fig. 3, is $z_{th} = 93.8$, close to the value observed. After the threshold, the soliton width (amplitude) increases (decreases) gradually. Radiation forms a pedestal behind the soliton in the t axis. Figure 4 compares the theoretical threshold value z_{th} with numerical results for different values of the initial pulse width. We vary both the pulse width and amplitude so that the initial pulse corresponds to the fundamental soliton [cf. Eq. (22)]. For the fundamental soliton $A_0 \sim 1/w_0$, then $Q = 2A_0^2 w_0 \sim 1/w_0$. Therefore, the threshold is proportional to the fourth power of the initial width as follows from Eq. (39) and is confirmed by numerical results in Fig. 4.

Thus, the perturbation analysis provides a quantitative description of the suppression of the self-frequency shift,

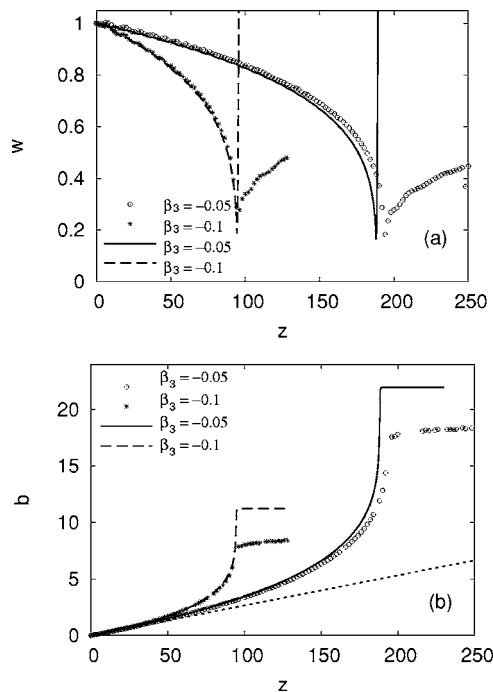


Fig. 2. Same as in Fig. 1 but for $\beta_3 < 0$.

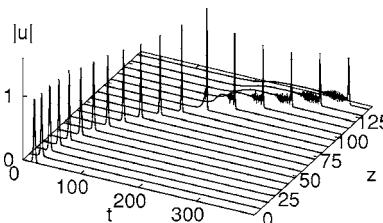


Fig. 3. Pulse evolution found from numerical simulations of Eq. (9). Parameters are $\beta_3 = -0.1$, $T_R = 0.05$, and $A_0 = w_0 = 1$.

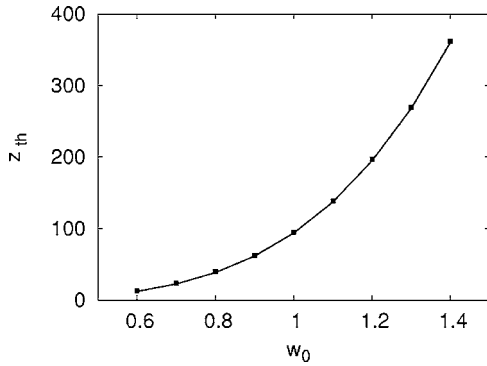


Fig. 4. Dependence of the threshold length on the soliton width. The curve corresponds to Eq. (39), and the points are from the numerical simulations of Eq. (9). Parameters are $\beta_3 = -0.1$, $T_R = 0.05$, and $A_0 = 1/w_0$.

which has been observed²² in PCFs for $\beta_3 < 0$ and studied theoretically.²³ The qualitative explanation of Skryabin and co-workers²² and Biancalana *et al.*²³ is as follows: A soliton generates dispersive waves (radiation) due to the higher-order effects. The radiation is redshifted for $\beta_3 < 0$. The interaction between the soliton and the resonant radiation results in a spectral recoil, which tends to blue-shift the soliton frequency. Since the Raman effect produces a redshift ($T_R > 0$), it can be suppressed by the spectral recoil. Our work here suggests that an important contribution to the suppression of the self-frequency shift is the energy loss by the soliton to resonant radiation. Note that by Eq. (27), this shift is proportional to the pulse energy Q . However, the decrease of the energy Q also results in an increase of the soliton width as seen from Eq. (36) and Fig. 2(a). Therefore, the rate of the frequency shift decreases since it is inversely proportional to w_s^4 [see Eq. (28)]. Also, as pointed out in Ref. 23, there is no complete cancellation of the Raman self-shift, because the soliton continues to transfer energy to radiation after the threshold.

We mention that for $\beta_3 \neq 0$, $T_S \neq 0$, and $T_R = 0$, considered in Subsection 4.D, Eqs. (29) and (30) also predict that $\hat{\beta}_2$ can approach close to zero. In that case, w_s can become very small; and, after that, $w(z)$ linearly increases without bound. However, such a situation can be realized for relatively large $T_S \gtrsim 0.3$ and $\beta_3 \gtrsim 0.3$ and for large deviation of the initial pulse from the fundamental soliton. Moreover, numerical simulations of Eq. (1) do not show such behavior. This difference is probably due to additional losses through radiation of linear waves.

F. General Case, $\beta_3 \neq 0$, $T_S \neq 0$, and $T_R \neq 0$

It is difficult to analyze the general case for an arbitrary set of parameters. The dynamics of w and b are found from Eqs. (12) and (17), respectively. As mentioned, the last equation describes the motion of an equivalent particle in a potential in addition to the dissipation or amplification effects. The minimum of the potential,

$$w_s = -\frac{2\hat{\beta}_2}{\gamma(1 - T_S b)Q} \quad (40)$$

changes on z . One can estimate the derivative:

$$\frac{dw_s}{dz} \approx \frac{2(\beta_3 - \beta_2 T_S)}{(1 - T_S b)^2 \gamma Q} b_z + O(\epsilon^2). \quad (41)$$

Then, assuming $b_z > 0$, $T_R > 0$, and $E_0 < 0$, we have

$$\begin{aligned} \frac{dw_s}{dz} &> 0, & \text{if } \beta_3 > \beta_2 T_S, \\ &< 0, & \text{if } \beta_3 < \beta_2 T_S. \end{aligned} \quad (42)$$

Then, the dynamics in the general case is similar to that described in Subsection 4.E but with a different threshold for parameter β_3 . In other words, the absolute value $|\beta_3|$ in the case $\beta_3 < 0$ should be large enough in order to observe the decrease of the pulse width and the threshold dynamics. We should mention that relation (42) is found from an asymptotic expansion, and therefore it is approximate. Nevertheless, it gives good estimates for the threshold on β_3 as has been confirmed by numerical simulations.

G. Parameters and Comparison

In this subsection, we discuss the range of the parameters where our results are valid. We also compare our theory with the previous analytical treatment.²³

A basic condition for the application of the perturbation approach is that the parameters defined in Eq. (10) are small. This condition is satisfied for many SC generation experiments reported recently. For example, the micro-structured optical fiber used by Ranka *et al.*⁶ has the following parameters, $\beta_2 \approx -4$ ps²/km, $\beta_3 \approx 0.06$ ps³/km, and $\gamma \approx 0.1$ /(mW) at the wavelength of 790 nm. The dispersion parameters were estimated from Fig. 2 of Ref. 6. For the pulse width $w_0 = 100$ fs, and taking $T_R = 3$ fs, one has $\bar{\beta}_3 = 0.15$ and $\bar{T}_S = 0.03$. In the experiment by Skryabin *et al.*,²² the PCF has $\beta_2 \approx -70$ ps²/km, $\beta_3 \approx -0.25$ ps³/km, and $\gamma = 0.12$ /(mW) for the core diameter ~ 1.2 μ m. Then, for the pulse width, $w_0 = 53$ fs, $\bar{\beta}_3 = 0.067$, and $\bar{T}_R = 0.057$. Therefore, in the experiments,^{6,22} the higher-order effects can be treated as small perturbations.

Another necessary condition is that the input pulse should be close to the fundamental soliton. The soliton peak power A_s^2 can be found from Eq. (22). This gives $A_s^2 \approx 4$ W for $w_s = 100$ fs for Ref. 6, and $A_s^2 \approx 250$ W for $w_s = 53$ fs for Ref. 22. These values of the peak power are close to those used in the experiments.^{6,22}

For the parameters mentioned above for Ref. 22 one finds from Eq. (39), that $z_{th} = 5$ m. The numerical modeling in Ref. 22 gives $z_{th} \approx 2.5$ m. An exact comparison is difficult because the parameters of the Raman effects are not specified in Ref. 22. In the numerical simulations of Ref. 23 $\bar{\beta}_2 = -1$, $\bar{\beta}_3 = -0.09$, $\gamma = 1$, and the Raman coefficient $\bar{T}_R = 0.012$. Then, for $A_s = 20^{1/2}$ and $w_s = 1/A_s$, Eq. (39) gives $z_{th} = 1.07$, which is quite close to the threshold value in Ref. 23.

As was mentioned in Section 1, the problem was also studied analytically in Ref. 23. The authors of Ref. 23 used a similar perturbation approach, but the radiation field was included explicitly. Moreover, an approximate formula for the radiation in the limit $z \rightarrow \infty$ was obtained. Then this expression was used in the adiabatic equations

for the soliton parameters Q and b . However, since the expression for radiation was taken at $z \rightarrow \infty$, the adiabatic expressions agree with the numerical modeling of the NLSE at large z , $z > z_{\text{th}}$. This is clearly seen in Fig. 4(b) of Ref. 23. In other words, the theory in Ref. 23 assumes that the role of radiation is the same at all z . In contrast, our approach gives a description for $z < z_{\text{th}}$ where the radiation is very small as follows from numerical simulations of the NLSE. Therefore, our theory and that in Ref. 23 provide mutually complementary results valid for different ranges of z or for different values of the initial pulse energy Q [see Eq. (39)].

5. CONCLUSIONS

We have studied the dynamics of solitons in optical fibers in the presence of the TOD, self-steepening, and Raman effects. Our approach is based on the method of moments.²⁴ We have justified the approach by comparing our results with those for the cases when the system is affected by the TOD or Raman effect only. We have found that the interplay of the high-order effect results in non-trivial dynamics of the soliton.

In particular, we demonstrated that the rate of the self-shift slowly decreases for positive TOD. This process occurs adiabatically without appreciable change of the soliton energy, due to the increase of the soliton width [see Eq. (27)]. The soliton spectrum moves away from the ZDP for $\beta_3 > 0$. Negative TOD also results in suppression of the frequency shift, though the dynamics differs from that for $\beta_3 > 0$. The frequency shift rate initially speeds up, and the soliton spectrum moves closer and closer to the ZDP. The soliton width decreases and the spectrum becomes wider. Near the ZDP, the soliton rapidly loses its energy to resonant radiation.^{22,23} Our theory is not valid after that point, because it does not account for such losses. However, this process results in the suppression of the frequency shift because of the spectral recoil from the induced radiation.^{22,23} Therefore, the self-shift suppression for $\beta_3 < 0$ involves both the soliton and the induced radiation. We show here that a potentially significant contribution to the weakening of the Raman effect is the reduction of the soliton energy. After the threshold, the Raman effect still pushes the soliton spectrum to the ZDP so that the soliton energy transfers continuously to radiation.

In addition to recent studies,^{21–23} we have considered the dynamics for the both signs of β_3 . The role of self-steepening is analyzed as well. We have obtained *explicit* relations for the soliton dynamics under the action of several effects. These relations are presented in Eqs. (31), (32), (36)–(39), and (42), giving the evolution of the soliton width, frequency shift, and velocity, as well as that of z_{th} . The soliton amplitude is found from Eq. (22).

The majority of the SC generation experiments^{4–8} have been performed in the *positive* β_3 region. As shown in Subsection 4.E, the pulse width increases with z for $\beta_3 > 0$, which means that the spectral width decreases. Therefore, the wide SC spectrum is not connected with wide spectra of individual solitons but is related to the balanced contribution of solitons with different central frequencies and the phase-matched radiation.

The region with $\beta_3 < 0$ can also be useful for SC generation, since the pulse width decreases for $\beta_3 < 0$, and therefore the pulse becomes spectrally wider. In fact, the SC generation in PCF with two zero dispersion points, so that $\beta_3 < 0$ for one of the points, was studied recently.^{32–34} However, our analysis shows that the system length should then be optimized with account of z_{th} . For $z < z_{\text{th}}$, the energy at the radiation frequency is small, while for $z > z_{\text{th}}$, the amount of energy at the soliton frequency decreases substantially. Therefore, to have a comparable contribution in the spectrum at the frequencies of the soliton and radiation, one needs to take the system length not much longer than z_{th} .

ACKNOWLEDGMENTS

This work was supported by the Australian Research Council under the ARC Centres of Excellence program.

E. N. Tsoy's e-mail address is etsoy@physics.usyd.edu.au.

*Also at Physical-Technical Institute of the Uzbek Academy of Sciences, Tashkent-84, Uzbekistan.

REFERENCES

1. G. P. Agrawal, *Nonlinear Fiber Optics* (Academic, 1995).
2. N. Akhmediev and A. Ankiewicz, *Solitons: Nonlinear Pulses and Beams* (Chapman & Hall, 1997).
3. A. I. Maimistov and A. M. Basharov, *Nonlinear Optical Waves* (Kluwer, 1999).
4. See, for example, R. R. Alfano, ed., *The Supercontinuum Laser Source* (Springer-Verlag, 1989).
5. See, for example, the special issue on supercontinuum generation, *Appl. Phys. B* **77**, A. Zheltikov, ed. (2003).
6. J. K. Ranka, R. S. Windeler, and A. J. Stentz, "Visible continuum generation in air silica microstructure optical fibers with anomalous dispersion at 800 nm," *Opt. Lett.* **25**, 25–27 (2000).
7. A. V. Husakou and J. Herrmann, "Supercontinuum generation of higher-order solitons by fission in photonic crystal fibers," *Phys. Rev. Lett.* **87**, 203901 (2001).
8. J. M. Dudley, L. Provino, N. Grossard, H. Maillotte, R. S. Windeler, B. J. Eggleton, and S. Coen, "Supercontinuum generation in air-silica microstructured fibers with nanosecond and femtosecond pulse pumping," *J. Opt. Soc. Am. B* **19**, 765–771 (2002).
9. A. Fuerbach, P. Steinvurzel, J. A. Bolger, and B. J. Eggleton, "Nonlinear pulse propagation at zero dispersion wavelength in anti-resonant photonic crystal fibers," *Opt. Express* **13**, 2977–2987 (2005).
10. R. K. A. Wai, C. R. Menyuk, Y. C. Lee, and H. H. Chen, "Nonlinear pulse-propagation in the neighborhood of the zero-dispersion wavelength of monomode optical fibers," *Opt. Lett.* **11**, 464–466 (1986).
11. F. M. Mitschke and L. F. Mollenauer, "Discovery of the soliton self-frequency shift," *Opt. Lett.* **11**, 659–661 (1986).
12. J. P. Gordon, "Theory of the soliton self-frequency shift," *Opt. Lett.* **11**, 662–664 (1986).
13. Yu. Kodama and A. Hasegawa, "Nonlinear pulse-propagation in a monomode dielectric guide," *IEEE J. Quantum Electron.* **23**, 510–524 (1987).
14. K. J. Blow and D. Wood, "Theoretical description of transient stimulated Raman-scattering in optical fibers," *IEEE J. Quantum Electron.* **25**, 2665–2673 (1989).
15. J. N. Elgin, T. Brabec, and S. M. J. Kelly, "A perturbative theory of soliton propagation in the presence of third-order dispersion," *Opt. Commun.* **114**, 321–328 (1995).

16. T. P. Horikis and J. N. Elgin, "Soliton radiation in an optical fiber," *J. Opt. Soc. Am. B* **18**, 913–918 (2001).
17. W. Zhao and E. Bourkoff, "Femtosecond pulse-propagation in optical fibers: higher-order effects," *IEEE J. Quantum Electron.* **24**, 365–372 (1987).
18. D. J. Frantzeskakis, K. Hizanidis, G. S. Tombras, and I. Bella, "Nonlinear dynamics of femtosecond optical solitary wave-propagation at the zero dispersion point," *IEEE J. Quantum Electron.* **31**, 183–189 (1995).
19. A. Ankiewicz, "Simplified description of soliton perturbation and interaction using averaged complex potentials," *J. Nonlinear Opt. Phys. Mater.* **4**, 857–870 (1995).
20. M. Golles, I. M. Uzunov, and F. Lederer, "Break up of N -soliton bound states due to intrapulse Raman scattering and third order dispersion—an eigenvalue analysis," *Phys. Lett. A* **231**, 195–200 (1997).
21. V. I. Karpman, "Radiation of solitons described by a high-order cubic nonlinear Schrödinger equation," *Phys. Rev. E* **62**, 5678–5687 (2000).
22. D. V. Skryabin, F. Luan, J. C. Knight, and P. St. J. Russell, "Soliton self-frequency shift cancelation in photonic crystal fibers," *Science* **301**, 1705–1708 (2003).
23. F. Biancalana, D. V. Skryabin, and A. V. Yulin, "Theory of the soliton self-frequency shift compensation by the resonant radiation in photonic crystal fibers," *Phys. Rev. E* **70**, 016615 (2004).
24. A. I. Maimistov, "Evolution of single waves close to solitons of Schrödinger nonlinear equation," *J. Exp. Theor. Phys.* **77**, 727 (1993) [*Zh. Eksp. Teor. Fiz.* **104**, 3620–3629 (1993)].
25. E. N. Tsoy, A. Ankiewicz, and N. Akhmediev, "Dynamical models for dissipative localized waves of the complex Ginzburg-Landau equation," *Phys. Rev. E* **73**, 036621 (2006).
26. W. L. Kath and N. F. Smith, "Soliton evolution and radiation loss for the nonlinear Schrödinger equation," *Phys. Rev. E* **51**, 1484–1492 (1995).
27. D. J. Kaup and A. C. Newell, "Exact solution for a derivative non-linear Schrödinger equation," *J. Math. Phys.* **19**, 798–801 (1978).
28. See, for example, B. A. Malomed, "Variational methods in nonlinear fiber optics and related fields," *Prog. Opt.* Vol. **43**, (Elsevier, 2002), pp. 71–193, and references therein.
29. F. Kh. Abdullaev and J. G. Caputo, "Validation of the variational approach for chirped pulses in fibers with periodic dispersion," *Phys. Rev. E* **58**, 6637–6648 (1998).
30. H. Goldstein, *Classical Mechanics* (Addison-Wesley, 1980).
31. J. Satsuma and N. Yajima, "Initial value-problems of one-dimensional self-modulation of nonlinear waves in dispersive media," *Prog. Theor. Phys. Suppl.* **55**, 284–306 (1974).
32. A. Efimov, A. J. Taylor, F. G. Omenetto, A. V. Yulin, N. Y. Joly, F. Biancalana, D. V. Skryabin, J. C. Knight, and P. S. J. Russell, "Time-spectrally-resolved ultrafast nonlinear dynamics in small-core photonic crystal fibers: experiment and modelling," *Opt. Express* **12**, 6498–6507 (2004).
33. K. M. Hilligsøe, T. V. Andersen, H. N. Paulsen, C. K. Nielsen, K. Mølmer, S. Keiding, R. Kristiansen, K. P. Hansen, and J. J. Larsen, "Supercontinuum generation in a photonic crystal fiber with two zero dispersion wavelengths," *Opt. Express* **12**, 1045–1054 (2004).
34. M. H. Frosz, P. Falk, and O. Bang, "The role of the second zero-dispersion wavelength in generation of supercontinua and bright-bright soliton-pairs across the zero-dispersion wavelength," *Opt. Express* **13**, 6181–6192 (2005).